Dalton Transactions

RSC Publishing

COMMUNICATION

View Article Online
View Journal | View Issue

Polyaniline nanorods dotted on graphene oxide nanosheets as a novel super adsorbent for Cr(VI)†

Cite this: *Dalton Trans.*, 2013, **42**, 7854

Received 16th January 2013,
Accepted 22nd March 2013

DOI: 10.1039/c3dt50149c

www.rsc.org/dalton

Shouwei Zhang,[a,b] Meiyi Zeng,[b] Wenqing Xu,[c] Jiaxing Li,*[a] Jie Li,[a] Jinzhang Xu[b] and Xiangke Wang[a]

Hierarchical nanocomposites of polyaniline (PANI) nanorods array on graphene oxide (GO) nanosheets are successfully obtained by dilute polymerization under −20 °C. They exhibit excellent water treatment performance with a superb removal capacity of 1149.4 mg g^{-1} for Cr(VI).

The rapid spread of heavy metal ion pollution in the environment has attracted much public attention due to their toxicity, high mobility and non-biodegradation.[1–4] Among the various kinds of heavy metal ions, the chromium (Cr(VI)) has been identified as one of the most toxic species owing to their carcinogenic, mutagenic to living organisms in biological systems.[5] The maximum permissible concentration of Cr(VI) ions in industrial wastewater is 0.25 mg L^{-1}, therefore, Cr(VI)-containing effluent must be treated before discharge.[4] To date, many approaches including adsorption, precipitation, electrodialysis, chemical coagulation–flocculation, membrane filtration, and ion exchange have been applied to remove Cr(VI) from wastewater.[6]

However, none of these methods are completely satisfactory and all feature the following disadvantages: (1) Generation of a large amount of secondary waste products due to various reagents used in a series of treatments such as reduction of Cr (VI), neutralization of acidic solution and precipitation. (2) Instability of ion-exchange resins due to serious oxidation by hexavalent chromium. Thus, the development of new, cost-effective, more environmentally friendly methods is needed.

Simultaneous adsorption and detoxification of Cr(VI) is considered as the most economical and effective method. However, conventional adsorbents often show a limited adsorption capacity or no reduction ability because they do not have enough surface area, functional groups and hydrophilic surface. Therefore, it is highly desirable to develop new nanomaterials with large surface area, high adsorption capacity and stability in extreme conditions.

By function-oriented selection of nanocomponents, hierarchical nanocomposites with high performance are highly expected and employed as adsorbents for the removal of heavy metal ions owing to their large specific surface areas and abundant functional groups. As one of the most important carbon family members, graphene oxide (GO) nanosheets have a unique two-dimensional structure and contain a large number of reactive oxygen-containing functional groups and high surface area (with a theoretical value of 2620 m^2 g^{-1}),[1] which render them a good candidate for supporting other functional nanomaterials, but they are easily agglomerated. The conducting polymer polyaniline (PANI) has good prospects in adsorption applications due to the positively charged nitrogen atoms in the polymer chains. Combining the unique properties of individual nanostructures and possibly synergistic effects, nanocomposites have attracted great attention in areas ranging from environmental applications to energy conversion and storage.[7] Therefore, conducting polymers and their combination with carbon-based derivatives have shown enhanced removal of mercury and other toxic pollutants from water.[8] However, most of the previous work focused on carbon-based polymer films that were difficult to prepare rapidly in large amounts. Also, films always have small specific surface areas, which may result in the relatively low activity because the reaction mainly occurs at the surface. In addition, bare PANI particles are easily aggregated in aqueous solutions, which lead to their relatively low adsorption capacity and slow kinetics, therefore limiting their adsorption capacity and practical application. Therefore, new nanomaterials with a superb removal capacity for heavy metal ions are still required for practical utility.

Herein, taking the advantages of PANI and the hydrophilic nature of GO, we reported a simple and novel hierarchical

[a]*Key Laboratory of Novel Thin Film Solar Cells, Institute of Plasma Physics, Chinese Academy of Sciences, 230031 Hefei, PR China. E-mail: lijx@ipp.ac.cn; Fax: +86-551-559-1310; Tel: +86-551-55-2788*

[b]*School of Materials Science and Engineering, Hefei University of Technology, Hefei 230031, China*

[c]*Department of Chemical Engineering, Environmental Engineering Program, Yale University, New Haven, Connecticut 06520, USA*

†Electronic supplementary information (ESI) available: Description of synthesis and characterization of the PANI/GO nanocomposite as well as the Cr(VI) adsorption experiment. See DOI: 10.1039/c3dt50149c

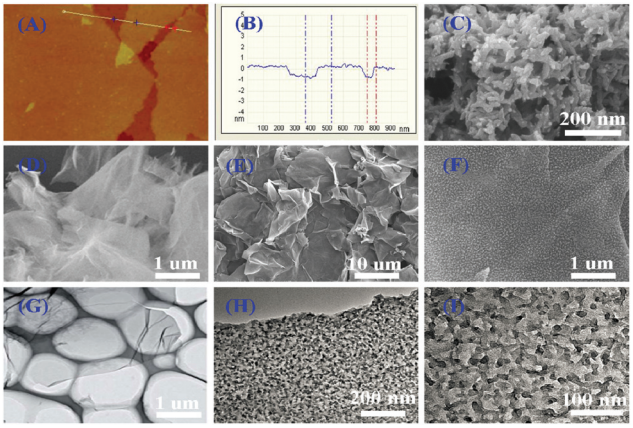

Fig. 1 AFM images of GO nanosheets on mica and its section analysis (A, B), SEM images of bare PANI nanorods (C), GO nanosheets (D), PANI/GO nanocomposites (E, F), TEM images of bare GO nanosheets (G), and PANI/GO nanocomposites (H, I).

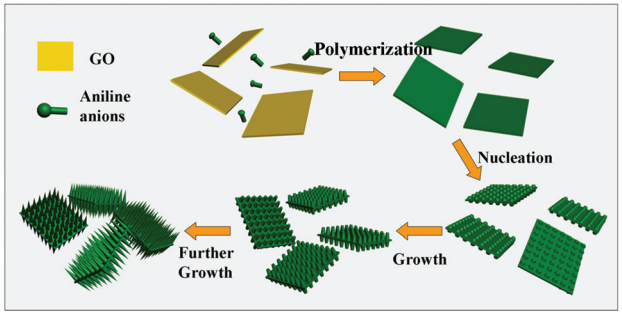

Fig. 2 Schematic illustration of nucleation and growth mechanism of aligned PANI nanorods on GO nanosheets.

nanocomposite of conducting PANI (1D nanorods) arrays grown vertically on GO (2D nanosheets). The hierarchical nanocomposites were synthesized by dilute polymerization in the presence of GO and aniline monomer (see ESI† for experimental details).

The AFM images (Fig. 1A and 1B) of GO nanosheets show the thickness of most GO nanosheets are *ca.* 1.0 nm for the individual GO nanosheets, which fit well with the thickness of an individual layer of GO.[1–3] The XRD, XPS and Raman characterizations further confirm the formation of GO nanosheets (Fig. S1, ESI†). The SEM image of PANI (Fig. 1C) shows disordered nanorods with small lengths (~70 nm). It is found that bare GO nanosheets are easily held together into agglomerates according to the SEM image (Fig. 1D) and possess a 2D nanosheet morphology with a size of several micrometers (Fig. 1G). Unlike the bare GO nanosheets, the PANI/GO nanocomposites do not form a stacking structure but show a free-standing sheet-like morphology with a thickness of ~160 nm (Fig. 1E and F). After decoration with PANI, the surface of GO nanosheets becomes rough and a lot of PANI nanorods uniformly cover the GO nanosheets (Fig. 1H and I), indicating that the nucleation and growth processes only occurred on the surface of GO nanosheets. This can be attributed to oxygen containing functional groups on the surface of GO nanosheets, which not only make GO nanosheets easily disperse in aqueous solution but also may act as the nucleation sites for PANI decoration.[6]

The randomly connected PANI nanorods from homogeneous nucleation in bulk solution and aligned PANI nanorods from heterogeneous nucleation on GO nanosheets, and the morphology of the hierarchical PANI/GO nanocomposites are also discussed (see Fig. S2, ESI†). On the basis of the above experimental results, a formation mechanism of PANI/GO nanocomposites is illustrated in Fig. 2. In the chemical oxidation polymerization process of PANI, two possible nucleation sites (that is, bulky solution and solid substrates) compete with each other. At the beginning of the chemical oxidation polymerization of PANI, a large amount of active sites were generated on the GO surface due to the electrostatic attraction between aniline ions and functional groups. As soon as $(NH_4)_2S_2O_8$ (APS) was added to the reaction system, aniline ions began to polymerize in these active sites and formed many tiny PANI protuberances on the nanosheets. These active sites would minimize the interfacial energy barrier between the solid surface and bulk solution, and moreover, they act as the "seeds" for the following polymerization. The low concentration of aniline cannot reach a supersaturation state so the homogeneous nucleation was suppressed. PANI nanorods would further grow along the initial nuclei, and therefore, aligned PANI nanorods on GO nanosheets were produced. However, when the concentration of aniline was higher, homogeneous nucleation would take place after the initial nucleation on the solid surface. Consequently, homogeneous nucleation would produce random connected PANI nanorods by using aniline micelles as "soft template".

As a result, two morphologies of PANI nanorods were produced, that is, random connected PANI nanorods from homogeneous nucleation in bulk solution and aligned PANI nanorods from heterogeneous nucleation on the GO nanosheets. However, because of the large specific area of the GO in the reaction system, the resultant PANI was more likely to form on the surface of GO.[9–11] The thickness of the PANI coating shell in PANI/GO nanocomposites was readily tunable by simply adjusting the mass ratio of aniline to GO in the fabrication processes (Fig. S3, ESI†)

The FTIR spectrum of GO (Fig. 3A) is typical for GO and consistent with previous work.[1–3] The absorption peaks at 3420, 1734, 1620, 1400, 1224 and 1100 cm^{-1} are attributed to the O–H, C=O in COOH, aromatic C=C, carboxy C–O, epoxy C–O and alkoxy C–O stretches, respectively.[1–3] Compared to GO, the FTIR spectrum of PANI/GO nanocomposites shows new absorption peaks at 1570 cm^{-1} (the aromatic C=C stretching of the quinonoid ring), 1490 cm^{-1} (the aromatic C=C stretching of the benzenoid ring), 1290 cm^{-1} (the C–N stretching of the secondary aromatic amine), 1230 cm^{-1} (the C–N^+ stretching), 1120 cm^{-1} (the =N^+–H stretching), and 795 cm^{-1} (the aromatic C–H out-of-plane deformation vibration) due to the existence of PANI nanorods.[7]

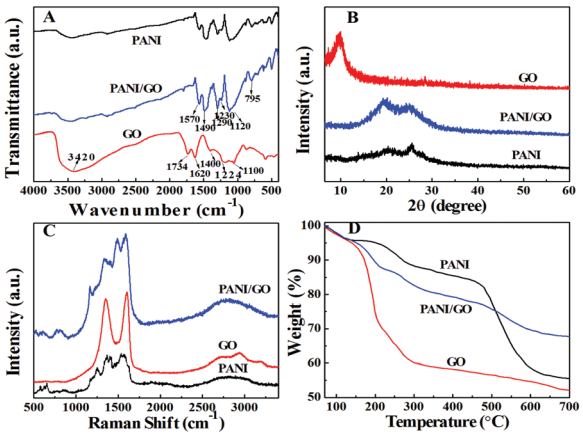

Fig. 3 FT-IR spectra (A), XRD patterns (B), Raman spectra (C), and TGA curves (D) of GO nanosheets, PANI nanorods, PANI/GO nanocomposites.

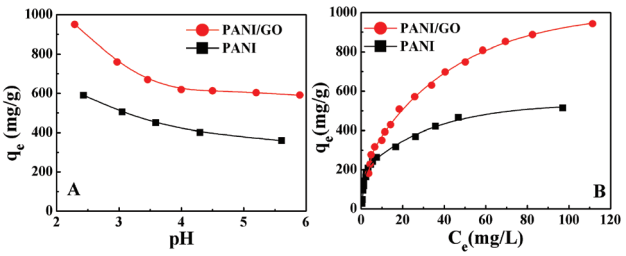

Fig. 4 Effect of pH on Cr(VI) removal by PANI nanorods and PANI/GO nanocomposites (the initial concentration of Cr(VI): 200 mg L^{-1}; adsorbent dose: 0.2 g L^{-1}; T = 25 °C) (A), Adsorption isotherms of Cr(VI) on PANI nanorods and PANI/GO nanocomposites (pH = 3; adsorbent dose: 0.2 g L^{-1}; T = 25 °C) (B).

XRD pattern of GO (Fig. 3B) reveals an intense, sharp peak centered at 2θ = 10.03°, corresponding to the interplanar spacing of 0.88 nm of GO nanosheets.[1–3] In the case of PANI/GO nanocomposites, the peak of GO stacking disappeared, indicating that the GO had almost no aggregation and was fully used as the substrate for the PANI nanorods to produce hierarchical nanocomposites. Two new broad peaks of PANI/GO nanocomposites centered at 2θ = 19.92° and 25.12° are almost the same as those of pure PANI nanorods, which are the characteristic Bragg diffraction peaks of PANI.[7]

As shown in Fig. 3C, the Raman spectrum of GO displays two prominent peaks at 1371 and 1627 cm^{-1}, corresponding to the well-documented D and G bands, respectively.[1–3] For the Raman spectrum of PANI/GO nanocomposites, apart from the D and G bands of GO, three new representative peaks arising from PANI can be indexed at 1516, 1184, and 819 cm^{-1}, which correspond to C=C stretching vibration of quinoid ring, C–H bending of the quinoid ring and substituted benzene ring deformation, respectively.[12] The new peaks also indicate the generation of PANI on the surfaces of GO. The results of Raman analysis are in good agreement with those of FTIR spectra analysis.

Fig. 3D shows the TGA curves of GO, PANI/GO and PANI. All the weight loss below 100 °C is attributed to the deintercalation of water. The dramatic weight loss from 160 to 300 °C in GO is resulted from the thermal decomposition of oxygen-containing groups.[13] Meanwhile, PANI shows a two-step weight loss from 200 to 600 °C due to the elimination of the doped acid bound to PANI chains and the decomposition of the pristine PANI backbone, respectively.[7] The TGA curve of PANI/GO nanocomposites is similar to a combination of that of GO and PANI, while the mass loss of PANI/GO from 100 to 700 °C is lower in comparison with those of GO and PANI. This can be understood by the fact that GO was partly reduced by aniline during the polymerization of PANI.

For Cr(VI) adsorption experiments, adsorbents were dispersed into Cr(VI) solution. After stirring for 4 h, the solution was filtered for Cr(VI) ions analysis (ESI†). The removal ability of the PANI/GO nanocomposites was found to be the highest when the mass ratio of aniline to GO was at about 9.3 : 1 or the thickness of the PANI coating shell was at about 80 nm (Fig. S4, ESI†).

The optimum range of the solution pH for the maximum removal of Cr(VI) by PANI/GO nanocomposites was investigated (Fig. 4A), and an optimal pH around 2.0–3.0 was observed. It is thus expected that the novel adsorbent (PANI/GO) can be applied in some extreme environments due to its high acidic resistance. The removal of Cr(VI) decreases with increasing solution pH, which is remarkably pH-dependent. The high removal efficiency at low pH can be attributed to the fact that at low pH values (1 < pH < 4), $HCrO_4^-$ is the major species of Cr(VI) (Fig. S7, ESI†).[14] The surface of PANI/GO is surrounded by abundant H^+. Therefore, the amine groups are easily protonated and positively charged, which favors the uptake of $HCrO_4^-$ through electrostatic attraction. An increase pH of solution will make the surface negatively charged, greatly weakening the electrostatic attraction between the adsorbent and negatively charged Cr(VI) anions, thus reducing the removal efficiency.

The adsorption isotherms of Cr(VI) are shown in Fig. 4B. The adsorption isotherms are fitted with Langmuir and Freundlich isotherm models, and the maximum adsorption capacities are calculated to be 490.2 mg g^{-1} for PANI and 1149.4 mg g^{-1} for PANI/GO nanocomposites (Table S1, ESI†). The PANI/GO nanocomposites exhibit a hierarchical structure and large surface area, and the presence of PANI prevents the stacking between the GO sheets and provides more functional groups. Therefore, PANI/GO nanocomposites are expected to have more adsorption sites for the binding of Cr(VI) ions and result in superb removal ability. Meanwhile, it was also found that the removal efficiency for Cr(VI) remained over 98% after five cycles, which indicated the feasibility of regenerating the PANI/GO nanocomposites (Fig. S6, ESI†). For comparison, the maximum adsorption capacities of Cr(VI) on PANI/GO nanocomposites and other adsorbents are listed in Table S3 (ESI†). One can see that the adsorption capability of the PANI/GO nanocomposites approaches 1149.4 mg g^{-1} for Cr(VI), which is the highest capability of today's nanomaterials. The adsorption kinetics of Cr(VI) on GO, PANI and PANI/GO nanocomposites are also discussed (see Fig. S5 and Table S2 and ESI†).

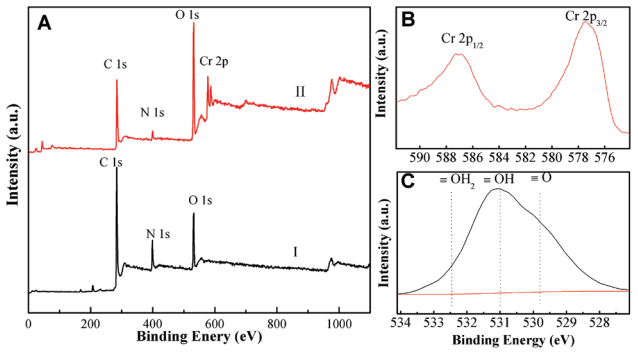

Fig. 5 The XPS spectra of PANI/GO nanocomposites: (I) before and (II) after Cr(VI) adsorption (A), high-resolution XPS Cr 2p (B) and O 1s (C) spectrum of PANI/GO nanocomposites after Cr(VI) adsorption (pH = 3, T = 25 °C).

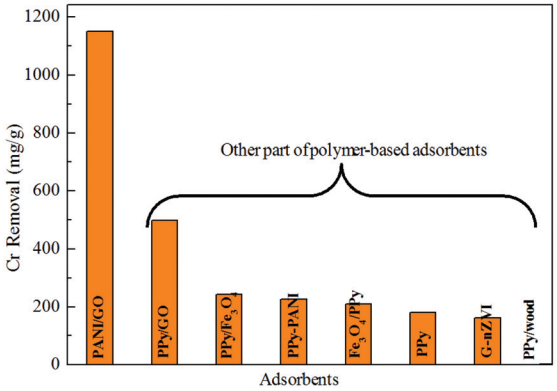

Fig. 6 Comparison of the sorption capacity of the hierarchical PANI/GO nanocomposites with other different adsorbents for Cr(VI) removal.

The XPS spectra of the PANI/GO nanocomposites before and after Cr(VI) adsorption are given in Fig. 5. Fig. 5A displays the presence of C, O, N and Cr components. Compared to the PANI/GO nanocomposites before Cr(VI) adsorption, two energy bands at about 577.5 eV and 587.2 eV corresponding to the binding energies of Cr $2p_{3/2}$ and Cr $2p_{1/2}$ are observed after Cr(VI) adsorption (Fig. 5B). The presence of Cr $2p_{3/2}$ proves the existence of the oxidation state of Cr(III). This result suggests that both Cr(III) and Cr(VI) exist on the surface of PANI/GO nanocomposites. It is easy to understand the existence of Cr(VI) species on the surface of PANI/GO nanocomposites. However, the presence of Cr(III) on the surface of PANI/GO nanocomposites indicates that some fraction of adsorbed Cr(VI) is reduced to Cr(III) during the adsorption process. The reduction phenomenon is due to the presence of positive nitrogen groups and the assistance of p electrons on the carbocyclic six-membered ring of PANI/GO.[15]

The results indicate that the PANI/GO nanocomposites are good candidates for Cr(VI) removal in one step by Cr(VI) adsorption coupled reduction into Cr(III). The existence of Cr(III) can be justified by the XPS survey for the oxygen 1s spectrum as shown in Fig. 5C. Asami and Hashimoto reported a comprehensive study on the oxygen 1s XPS scans for both Cr_2O_3 and $Cr(OH)_3$ with the former exhibiting a sharp peak at ~530 eV for $\equiv O^-$ and a small hump at ~532 eV for the adsorbed H_2O. In contrast, $Cr(OH)_3$ has a peak centering at ~531 eV for OH.[16]

A comparison of maximum adsorption capacity between PANI/GO nanocomposites and other nanomaterials reported in the literature has been presented in Fig. 6. It can be seen that the adsorption capacity of the PANI/GO nanocomposites is much higher than those materials.[17–23] The value is likely to be the highest among the adsorption data reported in the literature, and is significantly higher than those of many reported nanomaterials. The high adsorption capacity of Cr(VI) on PANI/GO nanocomposites makes them excellent candidates for potential applications in industrial wastewater treatment.

In summary, we have developed a simple and novel method for the synthesis of hierarchical PANI/GO nanocomposites using 1D (uniform aligned PANI nanorods) and 2D (GO nanosheets) nanocomponents by dilute polymerization. The synthesized PANI/GO nanocomposites are stable and environmentally friendly with a high Cr(VI) adsorption capacity of 1149.4 mg g^{-1} coupled with Cr(VI) reduction into Cr(III) species, advantageous over all polymer-based nanomaterials reported previously.

This work was supported by 973 project of MOST (2011CB933700), NNSF (21207136, 21272236, 21225730, 21077107), Natural Science Foundation of Anhui province (1208085QB32), Special Foundation for High-level Waste Disposal (2007-840) and Hefei Center for physical science and technology (2012FXZY005).

Notes and references

1 G. X. Zhao, L. Jiang, Y. D. He, J. X. Li, H. L. Dong, X. K. Wang and W. P. Hu, *Adv. Mater.*, 2011, **23**, 3959.
2 G. X. Zhao, X. M. Ren, X. Gao, X. L. Tan, J. X. Li, C. L. Chen, Y. Y. Huang and X. K. Wang, *Dalton Trans.*, 2011, **40**, 10945.
3 G. X. Zhao, J. X. Li, X. M. Ren, C. L. Chen and X. K. Wang, *Environ. Sci. Technol.*, 2011, **45**, 10454.
4 Y. Yuan, G. H. Zhang, Y. Li, G. L. Zhang, F. B. Zhang and X. B. Fan, *Polym. Chem.*, 2013, **4**, 2164.
5 N. Goyal, S. C. Jian and U. C. Banerjee, *Adv. Environ. Res.*, 2003, **7**, 311.
6 H. Jabeen, V. Chandra, S. Jung, J. W. Lee, K. S. Kim and S. B. Kim, *Nanoscale*, 2011, **3**, 3583.
7 J. J. Xu, K. Wang, S. Z. Zu, B. H. Han and Z. X. Wei, *ACS Nano*, 2010, **4**, 5019.
8 V. Chandra and K. S. Kim, *Chem. Commun.*, 2011, **47**, 3942.
9 L. Liang, J. Liu, C. F. Windisch, G. J. Exarhos and Y. Lin, *Angew. Chem., Int. Ed.*, 2002, **41**, 3665.
10 J. Liu, Y. H. Lin, L. Liang, J. A. Voigt, D. L. Huber, Z. R. Tian, E. Coker, B. Mckenzie and M. J. Mcdermott, *Chem.–Eur. J.*, 2003, **9**, 604.
11 N. R. Chiou, C. M. Lu, J. J. Guan, L. J. Lee and A. J. Epstein, *Nat. Nanotechnol.*, 2007, **2**, 354.
12 X. B. Yan, J. T. Chen, J. Yang, Q. J. Xue and P. Miele, *ACS Appl. Mater. Interfaces*, 2010, **2**, 2521.

13 M. Li, X. Y. Huang, C. Wu, H. P. Xu, P. K. Jiang and T. Tanaka, *J. Mater. Chem.*, 2012, **22**, 23477.
14 H. L. Ma, Y. W. Zhang, Q. H. Hu, D. Yan, Z. Z. Yu and M. L. Zhai, *J. Mater. Chem.*, 2012, **22**, 5914.
15 S. B. Deng and Y. P. Ting, *Environ. Sci. Technol.*, 2005, **39**, 8490.
16 K. Asami and K. Hashimoto, *Corros. Sci.*, 1984, **24**, 83.
17 R. Ansari and N. K. Fahim, *React. Funct. Polym.*, 2007, **67**, 367.
18 H. Jabeen, V. Chandra, S. Jung, J. W. Lee, K. S. Kim and S. B. Kim, *Nanoscale*, 2011, **3**, 3583.
19 Y. Q. Wang, B. F. Zou, T. Gao, X. P. Wu and S. Y. Lou, *J. Mater. Chem.*, 2012, **22**, 9034.
20 M. Bhaumik, A. Maity, V. V. Srinivasu and M. S. Onyango, *Chem. Eng. J.*, 2012, **181**, 323.
21 M. Bhaumik, A. Maity, V. V. Srinivasu and M. S. Onyango, *J. Hazard. Mater.*, 2011, **190**, 381.
22 S. K. Li, X. F. Lu, Y. P. Xue, J. Y. Lei, T. Zheng and C. Wang, *PLoS One*, 2012, **7**, e43328, DOI: 10.1371/journal.pone.0043328.
23 T. J. Yao, T. Y. Cui, J. Wu, Q. Z. Chen, S. W. Lu and K. N. Sun, *Polym. Chem.*, 2011, **2**, 2893.

